Spectrum of hot methane in astronomical objects using a comprehensive computed line list

Sergei N. Yurchenko[a,1], Jonathan Tennyson[a], Jeremy Bailey[b], Morgan D. J. Hollis[a], and Giovanna Tinetti[a]

[a]Department of Physics and Astronomy, University College London, London WC1E 6BT, United Kingdom; and [b]School of Physics, University of New South Wales, Sydney, NSW 2052, Australia

Edited by Mark H. Thiemens, University of California, San Diego, La Jolla, CA, and approved May 19, 2014 (received for review January 7, 2014)

Hot methane spectra are important in environments ranging from flames to the atmospheres of cool stars and exoplanets. A new spectroscopic line list, 10to10, for $^{12}CH_4$ containing almost 10 billion transitions is presented. This comprehensive line list covers a broad spectroscopic range and is applicable for temperatures up to 1,500 K. Previous methane data are incomplete, leading to underestimated opacities at short wavelengths and elevated temperatures. Use of 10to10 in models of the bright T4.5 brown dwarf 2MASS 0559-14 leads to significantly better agreement with observations and in studies of the hot Jupiter exoplanet HD 189733b leads to up to a 20-fold increase in methane abundance. It is demonstrated that proper inclusion of the huge increase in hot transitions which are important at elevated temperatures is crucial for accurate characterizations of atmospheres of brown dwarfs and exoplanets, especially when observed in the near-infrared.

Methane is an important terrestrial greenhouse gas (1) and the active component in many flames. It is also the major active atmospheric constituent of cool carbon stars, and the T-dwarf class of brown dwarfs which are often referred to as "methane dwarfs" (2, 3). Methane is also important for the newly discovered Y dwarfs (4), and even L dwarfs (5). Methane has been detected in exoplanets (6–8), where it has long been thought of as a potential biosignature (9, 10) on Earth-like planets. Equilibrium chemistry models for exoplanet gas giants (11) predict methane to be the main carbon containing species at temperatures below 1,500 K, so measuring its abundance is essential for determining the key C/O ratio in these objects (12, 13). Even though methane is therefore likely to be important in many of the giant exoplanets detected so far, its observed abundance remains controversial (14, 15). Studies of many topics, ranging from the astronomical ones just mentioned to halon flame inhibitors (16), combustion (17), gas turbine energies (18), and exhausts (19), all rely on an understanding of the spectroscopy of hot methane. However, even at room temperature the spectrum of methane is complex and not fully characterized (20). At elevated temperatures, above about 1,000 K, billions of spectral lines become active, and modeling hot methane with available laboratory data has often proved difficult (21, 22). The importance of an accurate and complete line list for methane has been stressed many times (23–26).

None of the available CH_4 line lists are complete at elevated temperatures (23). The recently updated CH_4 data (20) included in the 2012 edition of the high-resolution transmission molecular absorption database (HITRAN) (27) are designed to work at Earth atmosphere temperatures. Current high-temperature line lists include ones computed from first principles (28) and semiempirically (29) as well as (partial) experimental line lists (30–33). As demonstrated below, all of these compilations underestimate the number of methane transitions that need to be considered at elevated temperatures by many orders of magnitude.

Here we present a new methane line list computed variationally which contains 9.8 billion transitions and is designed to be complete for temperatures up to 1,500 K. It covers wavelengths from the far-infrared to 0.9 μm. This can be compared with about 340,000 transitions of $^{12}CH_4$ known experimentally for the same wavelength region. We show that proper inclusion of the huge increase in hot transitions which are important at elevated temperatures is crucial for accurate characterization of atmospheres of brown dwarfs and exoplanets, especially when observed in the near-infrared.

The 10to10 Line List

Methane has five atoms and hence nine vibrational modes, more than are routinely treated using variational nuclear motion programs. However, it is a highly symmetric molecule belonging to the $\mathcal{T}_d$ point group which allows some simplification. The rovibrational energies, associated wave functions, and Einstein A coefficients, which are required to generate spectra, were computed using a specifically adapted version of the nuclear motion program TROVE (34) in conjunction with a new spectroscopically obtained potential energy surface (PES) and a previously calculated, ab initio dipole moment surface (DMS) (35). The energies were computed variationally, i.e., by diagonalizing a large set of (200) Hamiltonian matrices constructed using a suitable basis set in the symmetry adapted representation. The largest matrix considered (for rotational state $J = 39$) had 163,034 × 163,034 elements and was diagonalized using the (nonsparse) scalable linear algebra package (ScaLAPACK) direct eigensolver PDSYEVR. A direct diagonalization of large nonsparse matrices is the bottleneck in variational computation of comprehensive line lists for polyatomic molecules. These calculations were performed at the UK National Cosmology Supercomputer COSMOS and required about 1.5M CPU hours. Calculating the line intensities is also computationally expensive but more straightforward; these calculations are independent and thus can be very efficiently parallelized. This part of the project was performed at The Cambridge

Significance

Hot methane is important in cool stars, brown dwarfs, exoplanets, gas turbine engines, and elsewhere. There is a pressing need for an accurate and complete spectroscopic database for methane at elevated temperatures. We present a comprehensive spectroscopic line list for methane containing almost 10 billion transitions, 2,000 times more than any previous compilation, covering a broad spectroscopic range and applicable for temperatures up to 1,500 K. We demonstrate that such a line list is essential for correctly modeling the brown dwarf 2MASS 0559-14 and leads to large changes in exoplanet models. We believe that this line list will have a large effect on the field of exoplanets and cool stars.

Author contributions: S.N.Y., J.T., and G.T. designed research; S.N.Y., J.T., J.B., M.D.J.H., and G.T. performed research; S.N.Y., J.T., J.B., M.D.J.H., and G.T. analyzed data; and S.N.Y., J.T., J.B., M.D.J.H., and G.T. wrote the paper.

The authors declare no conflict of interest.

This article is a PNAS Direct Submission.

Freely available online through the PNAS open access option.

[1]To whom correspondence should be addressed. E-mail: s.yurchenko@ucl.ac.uk.

This article contains supporting information online at www.pnas.org/lookup/suppl/doi:10.1073/pnas.1324219111/-/DCSupplemental.

High Performance Computing Cluster Darwin (3.0M CPU hours). Full details of the computational method used to construct the line list will be published elsewhere (36).

To reduce computational requirements, we imposed an upper energy limit of $E = hc$ 18,000 cm^{-1}. With this threshold for all rotational states up to $J = 39$, we obtained 6,603,166 energy levels. Einstein A coefficients were computed for all transitions involving rotational excitations $J = 0 \ldots 39$ with the lower and upper state energies ranging up to hc 8,000 cm^{-1} and hc 18,000 cm^{-1}, respectively, and covering the wavenumber range up to 12,000 cm^{-1} (0.83 μm). A total of 9,819,605,160 transitions were computed. The energy values, transition wavenumbers, Einstein A coefficients, and degeneracy factors compose our 10to10 line list, which can be obtained from www.exomol.com.

The large basis set used in the diagonalization plus the combination of an accurate variational model, an empirical PES, and ab initio DMSs obtained at the high level of ab initio theory (37) all contribute to the high quality of the 10to10 line list. Further technical details are given in *Supporting Information*. This line list forms a key part of the ExoMol project (26), which aims to provide such lists for all molecules likely to be detected in exoplanetary atmospheres.

Line List Results

Typical agreement with the experimental spectra is shown in Fig. 1, where the absorption intensities for the ν_3 (stretching asymmetric) band at $T = 296$ K are shown as a stick diagram. Not only do the theoretical line positions agree well with the measurements, but the absolute intensities reproduce the experimental data with an accuracy comparable to that of the experiment, where the latter is available. Validation by experiment is important because it gives us confidence in our predictions of the methane opacity. Indeed, our intensities are based purely on the quality of the ab initio DMS, without any empirical adjustments.

The 10to10 line list offers at least 200 times more lines than any other previous compilation, including the most complete: the empirically constructed methane calculated spectroscopic database (MeCaSDa) (29). Most of these extra transitions come from spectral lines which involve high rotational levels and/or transitions between vibrationally excited states (hot bands). These transitions are generally very weak in room-temperature spectra but become important when the temperature increases. To demonstrate the importance of these transitions we have counted the number of active transitions as a function of temperature. At room temperature, only 1% of the 10to10 lines have intensities stronger than 10^{-30} cm/molecule, which roughly corresponds to the scope of CH_4 in the HITRAN 2012 database (27). This shows that most 10to10 lines are unimportant for room temperature applications. However, at $T = 1{,}500$ K, 98% of 10to10 lines have absorption intensities stronger than 10^{-32} cm/molecule, 80% are stronger than 10^{-30}, and 40% are stronger than 10^{-29} cm/molecule. In addition, the density of these lines is extremely high, up to 66,000 lines per cm^{-1} at $T = 1{,}500$ K for the standard HITRAN cutoff of 10^{-29} cm/molecule. This means that billions of transitions are required to model the high temperature spectrum of methane.

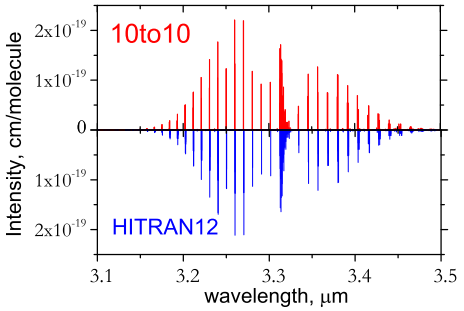

Fig. 1. Absorption intensities of the ν_3 band of $^{12}CH_4$ at $T = 296$ K: HITRAN (*Lower*) and 10to10 (*Upper*).

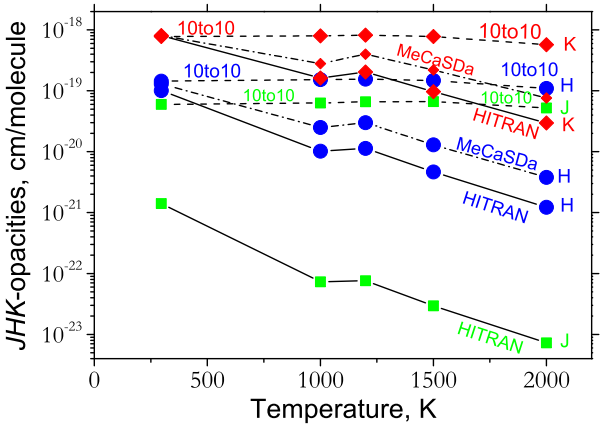

Fig. 2. Integrated intensities for the *K*, *H*, and *J* bands computed using different line lists: HITRAN 2012 (27), MeCaSDa (29), and 10to10. MeCaSDa gives the largest *K* and *H* coefficients for all of the previously available line lists but does not cover the *J* band, for which all previous line lists are very incomplete even at room temperature.

It is common astronomical practice to estimate the integrated flux within so-called *J*, *H*, *K*, *L*, *M* ... colors, or bands, which correspond to the transparency windows of the Earth atmosphere in the infrared. Here we present integrated opacities of CH_4 at different temperatures for the three main methane spectroscopic windows: the *J*, *H*, and *K* bands, which are defined as 1.1–1.4 μm, 1.5–1.8 μm, and 2.0–2.4 μm, respectively. Fig. 2 compares 10to10 integrated intensities with estimates obtained from the HITRAN and MeCaSDa databases. Agreement is good at room temperature for the *H* and *K*, but all previous compilations show a rapid drop in the methane opacity with temperature, whereas 10to10 suggests that it is approximately flat. The 10to10 line list gives enhanced absorption in the *J* band for all temperatures, which is to be expected because this region is poorly sampled experimentally (20). At high temperatures ($T > 1{,}500$ K), however, the 10to10 intensities deviate from a flat line, showing incompleteness of the 10to10 line list for such temperatures. To improve the temperature coverage to, say, 2,000 K, the lower energy threshold has to be also extended at least up to 10,000 cm^{-1}, and the rotational excitations have to be extended to about $J = 45$.

Astronomical Models

In Fig. 3 we present the results of modeling a spectrum of the bright T4.5 dwarf 2MASS 0559-14 taken from the Infrared Telescope Facility spectral library (39, 40). At this spectral type, methane bands at around 1.6 and 2.2 μm are becoming prominent features in the spectrum. Previous analyses of the spectrum of this object have derived effective temperatures in the range 1,000–1,200 K and gravities of log g (in cgs units) = 4.5–5.0 (41, 42). The model spectrum was calculated using the versatile software for transfer of atmospheric radiation (VSTAR) and the methods described by Bailey and Kedziora-Chudczer (22). The model is based on a pressure–temperature structure for effective temperature 1,200 K and log $g = 5$ (43) and assumes equilibrium chemistry. The new model also uses updated absorption coefficients for the H_2–H_2 collision induced absorption (CIA) (44). The blue spectrum in Fig. 3 corresponds to the previous model which used the spherical top data system (STDS) methane line list (45), a precursor to the recent MeCaSDa line list (29). The red spectrum is the new model using the 10to10 line list: The

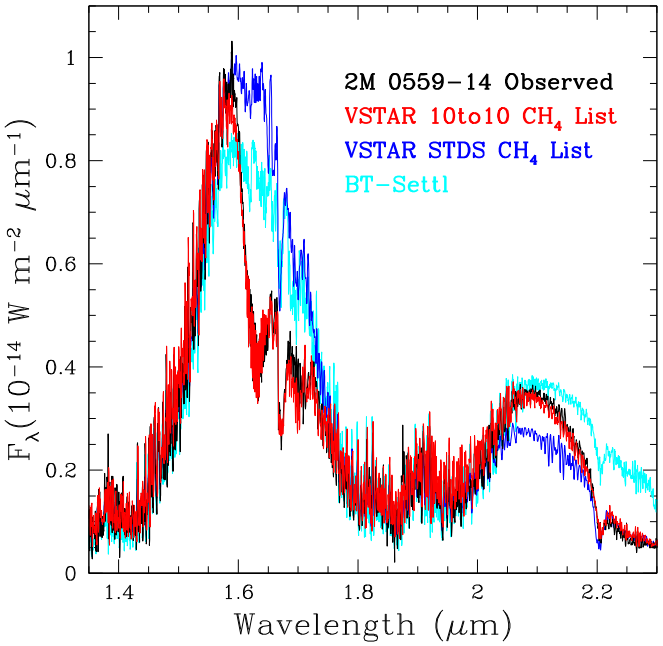

Fig. 3. VSTAR spectra of the T 4.5 dwarf: models are VSTAR with the 10to10 line list (this work), VSTAR with the STDS line list (22), and a comparison using the BT-Settl model of of Allard et al. (38). The observed spectrum was taken with the SpeX instrument on the 3-m NASA Infrared Telescope Facility (IRTF) and was obtained from the IRTF spectral library (39, 40). It has a spectral resolving power ($R = \lambda/\Delta\lambda$) of 2,000 and an S/N of better than 50.

comparison of the new VSTAR model using 10to10 with the old VSTAR model using the STDS list provides the direct comparison of the effect of just changing the opacities. Also included on the plot are results obtained using the BT-Settl model (38) for $T_{\rm eff}$ = 1,200 K and log g = 5, which is also based on the old line lists and similarly fails to match the observations in the regions of strong methane absorption.

It can be seen that the new model using the 10to10 list fits the data much better, particularly in the 1.6–1.8 μm region. In this region the STDS based lists used previously include no hot bands and clearly fail to properly represent the absorption in this region. Fig. 4 shows two expanded views of the spectral regions sensitive to methane and shows that much of the detailed line structure is reproduced by the model. The VSTAR model used here, which is a cloud-free model, fits the data for this object significantly better than the BT-Settl model, which includes clouds.

A line list as large as 10to10 presents something of a challenge for a line-by-line modeling code such as VSTAR. Initially, we tried to model the spectrum using a line intensity cutoff of 10^{-27} cm/molecule at 1,500 K to reduce the number of lines used in the line-by-line code. However, this procedure was found to produce significantly less absorption than the use of the full line list. Even though the lines below this cutoff are very weak, the very large number of them means they still contribute significant total absorption. To speed up the line-by-line calculations, we have divided the lines into strong and weak lines. Only the strong methane lines are modeled with a full line shape calculation. For the many weak lines we simply add the total line absorption into the single wavelength bin in which the line center lies. Given that there are many more lines than there are wavelength bins in our spectrum, these lines are clearly never going to be individually resolved. In the models presented here the boundary between strong and weak lines was set at 10^{-26} cm/molecule at the temperature of the atmospheric layer being modeled.

It remains very challenging to obtain even relatively crude spectra of exoplanets. The most productive technique has been monitoring the variation in observed starlight for those planets that transit their host star as viewed from Earth, for both the primary and secondary eclipse. Interpreting these observations requires the construction of detailed radiative transfer models. TAU (46, 47) is a one-dimensional radiative transfer code for transmission spectroscopy of exoplanets, especially designed for hot Jupiters with near-stellar orbits. It uses a line-by-line integration scheme to model transmission of the radiation from the parent star through the atmosphere of the orbiting planet, equating physically to observations of the radius ratio (transit depth) as a function of wavelength in the primary transit geometry. Abundances of absorbing molecules in the atmosphere can hence be estimated by hypothesizing compositions and comparing to any available observations. Specifically, the algorithm calculates the optical depth of the atmosphere (and hence effective radius of the planet) at a particular wavelength, given model trace molecular abundances and the atmospheric structure and absorbing behavior (in the form of line lists) of those molecules. A transit depth can hence be calculated as the ratio of the squared radii of the planet

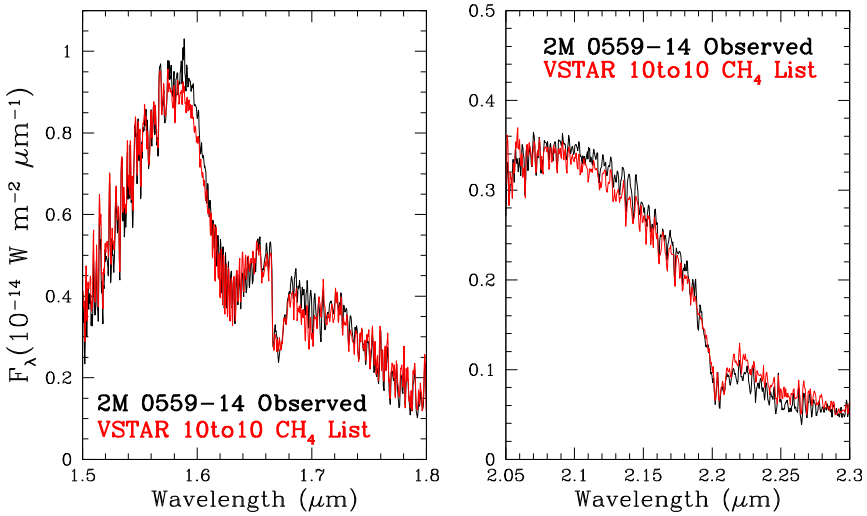

Fig. 4. Close up of spectra of the T 4.5 dwarf observed using IRTF compared with a VSTAR model with the 10to10 line list.

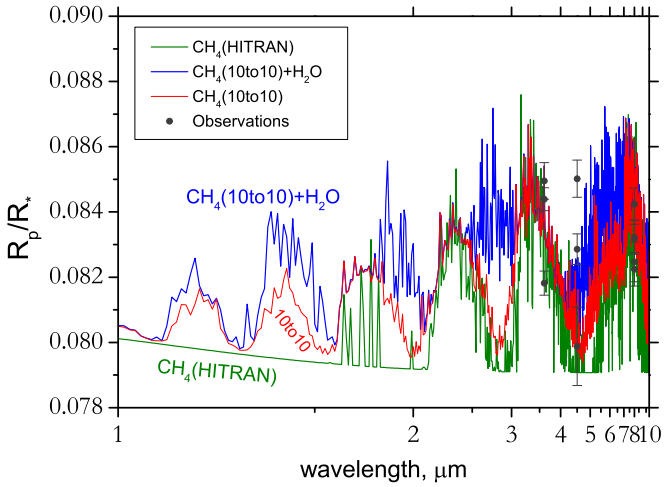

Fig. 5. TAU transmission spectra of the atmosphere of exoplanet GJ 436b at 700 K: 10to10 spectrum (methane only), HITRAN spectrum (methane only), and CH_4 (10to10) + water. Observation data are from Beaulieu et al. (15) and Knutson et al. (50). A mixing ratio of 10^{-5} for both H_2O and CH_4 was used. Note that recent observations in the 1.2–1.7 μm region indicate the presence of clouds or hazes (51) which are not included in our model.

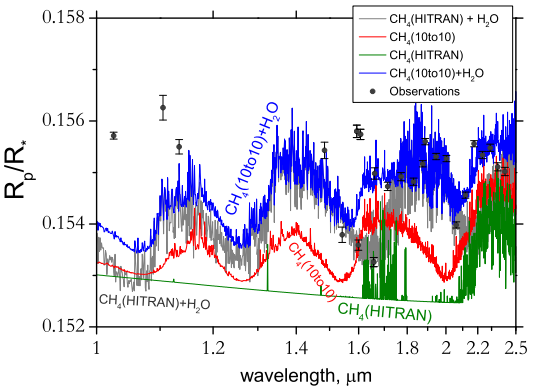

Fig. 6. TAU transmission spectra of the atmosphere of exoplanet HD 189733b at 1,000 K: 10to10 spectrum (methane only), experimental (HITRAN) spectrum (methane only), and the corresponding mixed H_2O + CH_4 spectra. The observations are a compilation of available measurements from refs. 6, 12, and 52–63. Mixing ratio is 5×10^{-4} for both H_2O and CH_4; the radius offset is 4.5%.

and the star, and a spectrum created of absorption as a function of wavelength.

We used TAU (46, 47) to generate models to simulate the atmospheric transmission of the warm Neptune GJ 436b (48) and of the hot Jupiter HD 189733b (49) (Figs. 5 and 6, respectively). Both these exoplanets have been extensively observed (6, 12, 15, 50–63). Assuming for GJ 436b an equilibrium temperature of about 700 K, the atmosphere of this planet is expected to contain significant quantities of methane as a trace absorber in chemical equilibrium (64–66) and some water. In models for GJ 436b containing only methane, the differences in the line lists result in an observed theoretical radius ratio increase $\Delta(R_p/R_*)$ of up to 0.3% at 5 μm and below 2 μm (after smoothing). Similar models on the well-studied exoplanet HD 189733b, a hot Jupiter with an effective temperature 1,200 K, found an increase of up to 0.6% (Fig. 6). If due solely to methane opacity, this would require an increase in modeled abundance of ~5 times using the HITRAN opacities to match the level predicted by 10to10. A large portion of these regions is, however, screened by water. This can be also seen in Figs. 5 and 6, where the results of the CH_4 + H_2O models are presented. In particular, the 5-μm regions are completely dominated by the water absorption, making the effect from the new methane data at this wavelength negligible. However, the windows around 1.6 μm and 2.2 μm show a significant difference with an increase of the radius ratio of up to 0.1% for the CH_4 (10to10) + H_2O model of the hot Jupiter HD 189733b in Fig. 6. The corresponding mixing ratios of CH_4 and H_2O were obtained by fitting to the observations available in the literature. In addition to the 10to10 and HITRAN 2012 line lists for methane, the BT2 line list (67) was used to model absorption by water. It should be noted that the large uncertainties of the existing observation data points, some of which appear to contradict each other (e.g., Fig. 5), lead to a very large number of possible solutions. Figs. 5 and 6 show only one selection of models as an example illustrating the significance of the potential errors involved in using line lists that are known to have missing opacities. These errors may not have been obvious in previous studies because the methane discrepancies are often masked to a large extent by the inclusion of realistic quantities of water at around the 10^{-5} abundance level.

Conclusion

We present a new comprehensive line list for methane suitable for modeling absorptions up to 1,500 K. An important consideration is that use of 10to10 increases opacities generated by methane, which changes the level of the atmosphere at which methane is absorbed or emitted. Future exoplanet models will have to account for the new opacities to retain self-consistency. The increased methane opacities are expected to have some effect on the pressure–temperature profile and thermal evolution of brown dwarfs and exoplanets. However, this is beyond the scope of the models considered here. Such effects can be properly evaluated when the new opacities are included in self-consistent structure models for the atmospheres and interiors. However, we would expect the changes to be relatively small as the extra opacity seen with the new line list is a relatively small fraction of the total opacity due to all sources, such as water, methane, and CIA.

Despite the size of the 10to10 line list it is still not complete. We can estimate the effect of the incompleteness of the 10to10 line list by comparison with the high-temperature partition function (68). The critical parameter here is the constraint introduced by our use of a lower energy threshold at hc 8,000 cm^{-1} on the states that can be thermally occupied. The partition function of CH_4 computed using 10to10 levels lying below this threshold suggests that at 1,500 K these sample about 85% of the total contribution. This means that 10to10 remains incomplete and that for higher temperatures an even larger number of lines will be required for accurate modeling of the opacity of methane in hot media such as exoplanets and (cool) stars.

ACKNOWLEDGMENTS. This work made extensive use of the high performance computing (HPC) systems Darwin and COSMOS as part of the DiRAC (Distributed Research Utilising Advanced Computing) facility. DiRAC is the UK HPC facility for particle physics, astrophysics, and cosmology and is supported by the Science and Technology Research Council (STFC) and the Department for Business Innovation and Skills (BIS) through the BIS National E-infrastructure capital Grant ST/J005673/1 and STFC Grants ST/H008586/1 and ST/K00333X/1. We thank University College London for use of the Legion High Performance Computer for performing the electronic structure calculations. This work was supported by the UK STFC, European Research Council Advanced Investigator Project 267219, and the Australian Research Council through Discovery Grant DP110103167.

1. Rhoderick GC, Dorko WD (2004) Standards development of global warming gas species: Methane, nitrous oxide, trichlorofluoromethane, and dichlorodifluoromethane. *Environ Sci Technol* 38(9):2685–2692.
2. Kirkpatrick JD (2005) New spectral types l and t. *Annu Rev Astron Astrophys* 43:195–245.
3. Burgasser AJ, Geballe TR, Leggett SK, Kirkpatrick JD, Golimowski DA (2006) A unified near-infrared spectral classification scheme for t dwarfs. *Astrophys J* 637(2):1067–1093.

4. Cushing MC, et al. (2011) The discovery of y dwarfs using data from the wide-field infrared survey explorer (WISE). *Astrophys J* 743(1):50.
5. Noll KS, Geballe TR, Marley MS (1997) Detection of abundant carbon monoxide in the brown dwarf gliese 229B. *Astrophys J* 489(1):L87–L90.
6. Swain MR, Vasisht G, Tinetti G (2008) The presence of methane in the atmosphere of an extrasolar planet. *Nature* 452(7185):329–331.
7. Swain MR, et al. (2010) A ground-based near-infrared emission spectrum of the exoplanet HD 189733b. *Nature* 463(7281):637–639.
8. Janson M, et al. (2011) Near-infrared multi-band photometry of the substellar companion GJ 758b. *Astrophys J* 728(2):85.
9. Sagan C, Thompson WR, Carlson R, Gurnett D, Hord C (1993) A search for life on Earth from the Galileo spacecraft. *Nature* 365(6448):715–721.
10. Atreya SK, Mahaffy PR, Wong AS (2007) Methane and related trace species on Mars: Origin, loss, implications for life, and habitability. *Planet Space Sci* 55(3):358–369.
11. Lodders K, Fegley B (2002) Atmospheric chemistry in giant planets, brown dwarfs, and low-mass dwarf stars: I. Carbon, nitrogen, and oxygen. *Icarus* 155(2):393–424.
12. Tinetti G, et al. (2007) Infrared transmission spectra for extrasolar giant planets. *Astrophys J* 654(1):L99–L102.
13. Madhusudhan N, et al. (2011) A high C/O ratio and weak thermal inversion in the atmosphere of exoplanet WASP-12b. *Nature* 469(7328):64–67.
14. Stevenson KB, et al. (2010) Possible thermochemical disequilibrium in the atmosphere of the exoplanet GJ 436b. *Nature* 464(7292):1161–1164.
15. Beaulieu JP, et al. (2011) Methane in the atmosphere of the transiting hot Neptune GJ436b? *Astrophys J* 731(1):16.
16. McNesby KL, Daniels RG, Miziolek AW, Modiano SH (1997) Optical measurement of toxic gases produced during firefighting using Halons. *Appl Spectrosc* 51(5):678–683.
17. Jourdanneau E, et al. (2007) CARS methane spectra: Experiments and simulations for temperature diagnostic purposes. *J Mol Spectrosc* 246(2):167–179.
18. Dinesh KKJR, Jenkins KW, Kirkpatrick MP, Malalasekera W (2009) Identification and analysis of instability in non-premixed swirling flames using LES. *Combustion Theory Modelling* 13(6):947–971.
19. Marran D, et al. (2001) Turbine engine exhaust gas measurements using in-situ FT-IR emission/transmission spectroscopy. *Proc SPIE* 4201:118–127.
20. Brown LR, et al. (2013) Methane line parameters in the HITRAN2012 database. *J Quant Spectrosc Radiat Transfer* 130:201–219.
21. Geballe TR, Kulkarni SR, Woodward CE, Sloan GC (1996) The near-infrared spectrum of the brown dwarf Gliese 229b. *Astrophys J* 467:L101–L104.
22. Bailey J, Kedziora-Chudczer L (2012) Modelling the spectra of planets, brown dwarfs and stars using VSTAR. *Mon Not R Astron Soc* 419(3):1913–1929.
23. Sharp CM, Burrows A (2007) Atomic and molecular opacities for brown dwarf and giant planet atmospheres. *Astrophys J Suppl Ser* 168(1):140–166.
24. Freedman RS, Marley MS, Lodders K (2008) Line and mean opacities for ultracool dwarfs and extrasolar planets. *Astrophys J Suppl Ser* 174:504–513.
25. Bailey J, Ahlsved L, Meadows VS (2011) The near-IR spectrum of Titan modeled with an improved methane line list. *Icarus* 213(1):218–232.
26. Tennyson J, Yurchenko SN (2012) ExoMol: Molecular line lists for exoplanet and other atmospheres. *Mon Not R Astron Soc* 425(1):21–33.
27. Rothman LS, et al. (2013) The HITRAN 2012 molecular spectroscopic database. *J Quant Spectrosc Radiat Transfer* 130:4–50.
28. Warmbier R, et al. (2009) Ab initio modeling of molecular IR spectra of astrophysical interest: application to CH_4. *Astron Astrophys* 495(2):655–661.
29. Ba YA, et al. (2013) MeCaSDa and ECaSDa: Methane and ethene calculated spectroscopic databases for the virtual atomic and molecular data centre. *J Quant Spectrosc Radiat Transfer* 130:62–68.
30. Nassar R, Bernath P (2003) Hot methane spectra for astrophysical applications. *J Quant Spectrosc Radiat Transfer* 82(1-4):279–292.
31. Thiévin J, et al. (2008) High-temperature emission spectroscopy of methane. *J Quant Spectrosc Radiat Transfer* 109(11):2027–2036.
32. Hargreaves RJ, Beale CA, Michaux L, Irfan M, Bernath PF (2012) Hot methane line lists for exoplanet and brown dwarf atmospheres. *Astrophys J* 757(1):46.
33. Campargue A, Leshchishina O, Mondelain D, Kassi S, Coustenis A (2013) An improved empirical line list for methane in the region of the $2\nu_3$ band at 1.66 μm. *J Quant Spectrosc Radiat Transfer* 118:49–59.
34. Yurchenko SN, Thiel W, Jensen P (2007) Theoretical rovibrational energies (TROVE): A robust numerical approach to the calculation of rovibrational energies for polyatomic molecules. *J Mol Spectrosc* 245(2):126–140.
35. Yurchenko SN, Tennyson J, Barber RJ, Thiel W (2013) Vibrational transition moments of CH_4 from the first principles. *J Mol Spectrosc* 291:69–76.
36. Yurchenko SN, Tennyson J (2014) Exomol line lists IV: The rotation-vibration spectrum of methane up to 1500 K. *Mon Not R Astron Soc* 440(2):1649–1661.
37. Nikitin AV, Rey M, Tyuterev VG (2013) New dipole moment surfaces of methane. *Chem Phys Lett* 565:5–11.
38. Allard F, et al. (2007) K-H_2 quasi-molecular absorption detected in the T-dwarf epsilon Indi Ba. *Astron Astrophys* 474:L21–L24.
39. Cushing MC, Rayner JT, Vacca WD (2005) An infrared spectroscopic sequence of M, L, and T dwarfs. *Astrophys J* 623(2):1115–1140.
40. Rayner JT, Cushing MC, Vacca WD (2009) The infrared telescope facility (IRTF) spectral library: Cool stars. *Astrophys J Suppl Ser* 185(2):289–432.
41. Stephens DC, et al. (2009) The 0.8-14.5 μm spectra of mid-L to mid-T dwarfs: Diagnostics of effective temperature, grain sedimentation, gas transport, and surface gravity. *Astrophys J* 702:154–170.
42. del Burgo C, Martin EL, Zapatero Osorio MR, Hauschildt PH (2009) Physical parameters of T dwarfs derived from high-resolution near-infrared spectra. *Astron Astrophys* 501:1059–1071.
43. Burrows A, Sudarsky D, Hubeny I (2006) L and T dwarf models and the L to T transition. *Astrophys J* 640:1063–1077.
44. Abel M, Frommhold L, Li X, Hunt KLC (2011) Collision-induced absorption by H2 pairs: From hundreds to thousands of kelvin. *J Phys Chem A* 115(25):6805–6812.
45. Wenger C, Champion JP (1998) Spherical top data system (STDS) software for the simulation of spherical top spectra. *J Quant Spectrosc Radiat Transfer* 59(3-5):471–480.
46. Tinetti G, Tennyson J, Griffith CA, Waldmann I (2012) Water in exoplanets. *Philos Trans A Math Phys Eng Sci* 370(1968):2749–2764.
47. Hollis MDJ, Tessenyi M, Tinetti G (2013) TAU: A 1D radiative transfer code for transmission spectroscopy of extrasolar planet atmospheres. *Comput Phys Commun* 184(10): 2351–2361.
48. Butler RP, et al. (2004) A Neptune-mass planet orbiting the nearby M dwarf GJ 436. *Astrophys J* 617(1):580–588.
49. Bouchy F, et al. (2005) ELODIE metallicity-biased search for transiting Hot Jupiters II. A very hot Jupiter transiting the bright K star HD189733. *Astron Astrophys* 444(1): L15–L19.
50. Knutson HA, et al. (2011) A Spitzer transmission spectrum for the exoplanet GJ 436b, evidence for stellar variability, and constraints on dayside flux variations. *Astrophys J* 735(1):27.
51. Knutson HA, Benneke B, Deming D, Homeier D (2014) A featureless transmission spectrum for the Neptune-mass exoplanet GJ 436b. *Nature* 505(7481):66–68.
52. Tinetti G, et al. (2007) Water vapour in the atmosphere of a transiting extrasolar planet. *Nature* 448(7150):169–171.
53. Knutson HA, et al. (2007) A map of the day-night contrast of the extrasolar planet HD 189733b. *Nature* 447(7141):183–186.
54. Sing DK, et al. (2009) Transit spectrophotometry of the exoplanet HD 189733b I. Searching for water but finding haze with HST NICMOS. *Astron Astrophys* 505(2): 891–899.
55. Desert JM, et al. (2009) Search for carbon monoxide in the atmosphere of the transiting exoplanet HD 189733b. *Astrophys J* 699(1):478–485.
56. Knutson HA, et al. (2009) Multiwavelength constraints on the day-night circulation patterns of HD 189733b. *Astrophys J* 690(1):822–836.
57. Agol E, et al. (2010) The climate of HD 189733b from fourteen transits and eclipses measured by Spitzer. *Astrophys J* 721(2):1861–1877.
58. Sing DK, et al. (2011) Hubble Space Telescope transmission spectroscopy of the exoplanet HD 189733b: High-altitude atmospheric haze in the optical and near-ultraviolet with STIS. *Mon Not R Astron Soc* 416(2):1443–1455.
59. Desert JM, et al. (2011) Transit spectrophotometry of the exoplanet HD 189733b II. new spitzer observations at 3.6 μm. *Astron Astrophys* 526(2):A12.
60. Gibson NP, et al. (2012) Probing the haze in the atmosphere of HD 189733b with Hubble Space Telescope/WFC3 transmission spectroscopy. *Mon Not R Astron Soc* 422(1):753–760.
61. Gibson NP, et al. (2012) A Gaussian process framework for modelling instrumental systematics: Application to transmission spectroscopy. *Mon Not R Astron Soc* 419(3): 2683–2694.
62. Pont F, et al. (2013) The prevalence of dust on the exoplanet HD 189733b from Hubble and Spitzer observations. *Mon Not R Astron Soc* 432(4):2917–2944.
63. Danielski C, et al. (2014) 0.94–2.42 μm ground-based transmission spectra of the hot Jupiter HD-189733b. *Astrophys J* 785(1):35.
64. Burrows A, Sharp CM (1999) Chemical equilibrium abundances in brown dwarf and extrasolar giant planet atmospheres. *Astrophys J* 512(2):843–863.
65. Moses JI, et al. (2013) Compositional diversity in the atmospheres of hot Neptunes, with application to GJ 436b. *Astrophys J* 777(1):34.
66. Venot O, Agundez M, Selsis F, Tessenyi M, Iro N (2014) The atmospheric chemistry of the warm Neptune GJ 3470b: Influence of metallicity and temperature on the CH_4/CO ratio. *Astron Astrophys* 562:A51.
67. Barber RJ, Tennyson J, Harris GJ, Tolchenov RN (2006) A high accuracy computed water line list. *Mon Not R Astron Soc* 368(3):1087–1094.
68. Wenger C, Champion JP, Boudon V (2008) The partition sum of methane at high temperature. *J Quant Spectrosc Radiat Transfer* 109(16):2697–2706.